HHS Public Access

Author manuscript

Neuroscience. Author manuscript; available in PMC 2018 January 11.

Published in final edited form as:

Neuroscience. 2017 October 11; 361: 179–191. doi:10.1016/j.neuroscience.2017.08.015.

LOSS OF SESTRIN 2 POTENTIATES THE EARLY ONSET OF AGE-RELATED SENSORY CELL DEGENERATION IN THE COCHLEA

CELIA ZHANG[a], **WEI SUN**[a], **JI LI**[b], **BINBIN XIONG**[a], **MITCHELL D. FRYE**[a], **DALIAN DING**[a], **RICHARD SALVI**[a], **MI-JUNG KIM**[c], **SHINICHI SOMEYA**[c], and **BO HUA HU**[a,*]

[a]Center for Hearing and Deafness, Department of Communicative Disorders and Sciences, State University of New York at Buffalo, 137 Cary Hall, Buffalo, NY 14214, USA

[b]University of Mississippi Medical Center, Department of Physiology and Biophysics, University of Mississippi, 2500 North State Street, Jackson, MS 39216, USA

[c]Departments of Aging and Geriatric Research, College of Medicine, University of Florida, 1600 SW Archer Road, Gainesville, FL 32610, USA

Abstract

Sestrin 2 (SESN2) is a stress-inducible protein that protects tissues from oxidative stress and delays the aging process. However, its role in maintaining the functional and structural integrity of the cochlea is largely unknown. Here, we report the expression of SESN2 protein in the sensory epithelium, particularly in hair cells. Using C57BL/6J mice, a mouse model of age-related cochlear degeneration, we observed a significant age-related reduction in SESN2 expression in cochlear tissues that was associated with early onset hearing loss and accelerated age-related sensory cell degeneration that progressed from the base toward the apex of the cochlea. Hair cell death occurred by caspase-8 mediated apoptosis. Compared to C57BL/6J control mice, *Sesn2* KO mice displayed enhanced expression of proinflammatory genes and activation of basilar membrane macrophages, suggesting that loss of SESN2 function provokes the immune response. Together, these results suggest that *Sesn2* plays an important role in cochlear homeostasis and immune responses to stress.

Keywords

sestrin 2 (SESN2); age-related hearing loss; cochlea; outer hair cells; macrophages; inflammation

INTRODUCTION

Sestrins are a family of highly conserved stress-responsive proteins that are inducible in cells exposed to stress (Lee et al., 2010). Mammalian tissues express three types of sestrins (sestrin 1, sestrin 2 and sestrin 3) (Lee et al., 2010) and these proteins are transcriptionally regulated by p53 and forkhead transcription factors (Budanov et al., 2010). The discovery of

*Corresponding author. Address: Center for Hearing and Deafness, University at Buffalo, 137 Cary Hall, 3435 Main Street, Buffalo, NY 14214, USA.

sestrins as p53 targets suggests that these proteins are stress-inducible and can modulate tissue response to stress (Budanov et al., 2002; Velasco-Miguel et al., 1999). Sestrins protect cells from various stresses, such as DNA damage, oxidative stress and hypoxia (Lee et al., 2013). They act as antioxidants that control the activity of peroxiredoxins by scavenging reactive oxygen species (ROS). At the cellular level, disruption of sestrin expression compromises metabolic processes, which causes oxidative stress, fat accumulation, and mitochondrial dysfunction, resembling an accelerated aging process in tissues (Lee et al., 2013). Because sestrin-targeted molecules are associated with age-related tissue pathogeneses (Finkel and Holbrook, 2000; Kapahi and Zid, 2004; Stanfel et al., 2009) and because sestrins protect tissues from a range of age-related diseases (Budanov and Karin, 2008; Budanov et al., 2004; Lee et al., 2010), we hypothesize that sestrins play a role as anti-aging molecules in the auditory system.

Age-related hearing loss (ARHL), one of the most common disorders in the elderly, is predominately associated with sensory cell degeneration. Approximately 25% of individuals between the ages of 50 and 65 years have hearing thresholds greater than 30 dB and self-reported hearing loss can be identified in 50% of those over the age of 85 (Liu and Yan, 2007). ARHL affects both the peripheral and central auditory systems, leading to elevation of hearing thresholds and deterioration of auditory processing functions (Frisina et al., 2001; Khullar and Babbar, 2011; Ohlemiller and Frisina, 2008). The magnitude of hearing dysfunction is affected by an individual's genetic background and lifetime insults to their auditory organ (Bielefeld et al., 2010; Ohlemiller, 2009). As age increases, the ability of the cochlea to tolerate stress decreases increasing susceptibility to ARHL.

Among the known biological changes that occur with aging, oxidative stress has been known as one of the key protagonists in the pathophysiology of ARHL. Aged cochleae display increased production of free radicals, a byproduct of aerobic metabolism (Sohal and Weindruch, 1996) and weakened antioxidant capacity (Jiang et al., 2007; Staecker et al., 2001; Tadros et al., 2014; Tanaka et al., 2012). While ROS can function as biological molecules for many physiological processes (Sena and Chandel, 2012), excessive ROS is toxic to cells and causes apoptosis (Kamogashira et al., 2015; Linehan and Fitzgerald, 2015; Orr and Sohal, 1994; Someya and Prolla, 2010). Moreover, ROS activities can interact with other pathological activities, such as inflammatory responses to potentiate the age-related sensory cell degeneration.

Sestrin 2 (SESN2), a key member of the sestrin family, has been investigated in the heart of aging mice (Morrison et al., 2015; Quan et al., 2017)and in colorectal cancer in human and murine populations (Ro et al., 2016; Wei et al., 2015). SESN2 is crucial during myocardial ischemia to promote AMPK activation and regulate cellular energy homeostasis (Morrison et al., 2015), suggesting a role for SESN2 in the AMPK signaling pathway. Decreased SESN2 expression in human colorectal cancer tissues is associated with poor prognosis (Wei et al., 2015). This has been attributed to overproduction of ROS, which are genotoxic, tumor progression and metastasis (Lee and Kang, 2013; Waris and Ahsan, 2006; Wei et al., 2015). SESN2 acts as a tumor suppressor in the colon; the colon of *Sesn2* knockout (KO) mice was more prone to inflammation (Ro et al., 2016). Additionally, patients with chronic colon inflammation have elevated levels of SESN2, whereas patients with colon cancer have very

low levels of SESN2 (Wei et al., 2015). Despite the importance of SESN2 in other fields, little is known about its functional roles in cochlear homeostasis and pathogenesis.

To investigate the function of SESN2 in cochlear sensory cell homeostasis and age-related degeneration, we assessed the expression of SESN2 in the sensory epithelium of mouse cochleae. SESN2 was downregulated with age. Importantly, loss of SESN2 function accelerated age-related sensory cell degeneration and auditory dysfunction. Cochlear pathogenesis was accompanied by enhanced inflammatory activity. Our study implicates SESN2 in sensory cell integrity and pathogenesis.

EXPERIMENTAL PROCEDURES

Animals and genotyping

Sesn2 KO mice (male and female) backcrossed for at least 9 generations with C57BL/6J mice were compared to C57BL/6J mice to determine how the deletion of the SESN2 protein affects the ARHL and hair cell degeneration. *Sesn2* KO mice, developed on the C57BL/6J background were generated in the Laboratory of Gene Regulation and Signal Transduction of the Department of Pharmacology at University of California, San Diego, La Jolla, CA, USA (Budanov and Karin, 2008). The *Sesn2* KO breeder mice provided by Dr. Ji Li (University of Mississippi Medical Center, Department of Physiology and Biophysics) were backcrossed to C57BL/6J mice for at least 9 generations (personal communication, Dr. Ji Li and Dr. Michael Karin, University of California, San Diego). C57BL/6J mice (The Jackson Laboratory, Bar Harbor, ME, USA) were used as controls. Because the C57BL/6J strain is homozygous for a recessive AHL-susceptibility allele $Cdh23^{753A}$, we confirmed that C57BL/6J controls and *Sesn2 KO* mice have the same genotype for *Cdh23.* Briefly, DNA from the tails of these mice was amplified using PCR and the region of DNA containing the 753rd nucleotide in the *Cdh23* gene was sequenced ($n = 3$). The following primers were used for PCR: Cdh23-F 5′-GATCAAGACAAG ACCAGACCTCTGTC-3′; Cdh23-R 5′ GAGCTACCAG GAACAGCTTGGGCCTG-3′. The size of amplified PCR product was 360 bps. We confirmed that all the C57BL/6J control and *Sesn2* KO mice had the same $Cdh23^{753A/753A}$ genotype (Fig. 1).

74 animals were used in this study (30 *Sesn2* KO mice and 44 C57BL/6J control mice). The KO and C57BL/6J control animals were divided into three age groups: 4–6 weeks, 3 months and 5 months. We limited the age range of the mice to 5 months because the C57BL/6J control mice develop significant high-frequency hearing loss after the age of 5 months (Someya et al., 2009) that could complicate the interpretation of the results. Both cochleae of each mouse were collected and processed for different experimental tests. The numbers of animals used in each experimental condition are presented in the Results section. All procedures involving the use and care of the animals were approved by the University at Buffalo Institutional Animal Care and Use Committee.

Auditory brainstem responses (ABR)

ABRs were measured to assess the auditory function of the mice. All ABR measurements were performed in a soundproof booth. Prior to testing, the animals were given

intraperitoneal injection of an anesthesia cocktail comprised of ketamine (100 mg/kg) and xylazine (10 mg/kg). Stainless steel electrodes were inserted subdermally over the vertex (active), posterior to the stimulated (reference) and non-stimulated (ground) ears of the animal. During the testing, the animal's body temperature was maintained at 37.5 °C using a heating system (Homeothermic Blanket Control Unit, Harvard Apparatus, Holliston, MA, USA).

The acoustic signals were generated and the responses were processed using Tucker-Davis Technologies (TDT, Alachua, FL, USA) hardware and software. The sound levels were calibrated using a sound level meter (824, Larson Davis, ø″ microphone). The electrodes used for ABR recordings were connected to a preamplifier (RA16LA, TDT) using a flexible, low-noise cable. The output of the preamplifier was sent to a digital signal processing module (RX5-2, Pentusa Base Station, TDT) and collected by software (BioSigRP, TDT). The ABRs were elicited with tone bursts of 4, 8, 16, 32 and 48 kHz. The average response to 1000 stimuli was obtained over a range of intensities at each frequency. The stimulus was initially presented at high intensities and decreased in 10-dB steps and then reduced in 5-dB steps near the threshold. Threshold was defined as the lowest intensity that reliably elicited a detectable response.

Immunolabeling

Immunostaining was performed to examine SESN2 protein expression in the organ of Corti and to identify basilar membrane macrophages. Animals were sacrificed and the cochleae were quickly removed from the skull, fixed with 10% buffered formalin, and dissected in 10 mM phosphate-buffered saline (PBS). The tissues were permeabilized with 0.5% Triton X-100 in 10 mM PBS for 30 min at room temperature. Specimens were incubated overnight at 4 °C with a rabbit polyclonal antibody against SESN2 (1.5:100, 10795-1-AP, Proteintech Group, Inc., Rosemont, IL, USA) or a goat polyclonal antibody against CD45 (1:200, AF114, R&D Inc., Minneapolis, MN, USA). After incubation with the primary antibodies, the tissues were rinsed three times with 10 mM PBS and incubated with a secondary antibody, Alexa Fluor 488 goat anti-rabbit IgG (H + L) (1.5:100 in PBS, Invitrogen, Carlsbad, CA, USA) or Alexa Fluor 488 donkey anti-goat IgG (1:200 in PBS, Life Technologies, Grand Island, NY, USA), for two hours at room temperature. After incubation, the samples were rinsed three times with PBS. In our previous studies, the specificity of the SESN2 primary antibody was confirmed using immunoblotting in C57BL/6J heart tissues (Morrison et al., 2015). The specificity of the CD45 primary antibody was verified by Western blot analysis in cochlear tissues (Cai et al., 2014a).

Assessment of sensory cell damage

The number of missing sensory cells in the organs of Corti was quantified using phalloidin staining of the cochlear tissues. The animals were decapitated under CO_2 gas anesthesia. The cochleae were extracted and fixed with 10% buffered formalin at 4 °C overnight. Then, the cochleae were dissected and the organs of Corti were collected. The tissues were stained with Alexa Fluor 488 or 594-labeled phalloidin (1:75, Applied Biosystems, Foster City, CA, USA) in 10 mM PBS for 20 min at room temperature. After staining, tissues were rinsed in PBS and then imaged using a fluorescence microscope (Leica Z6 APO Manual MacroFluo,

10× objective) equipped with a Leica DFC digital camera. Using Adobe Photoshop CS6, sections of individual images were aligned and the images of different layers were blended to generate a merged view of the tissue.

The images were visually inspected. Absence of phalloidin staining at the location of the hair cell cuticular plate was used as our criterion for a missing hair cell. The pattern of sensory cell damage was determined by quantifying the number of missing outer hair cells (OHCs) along the sensory epithelium from the apex to the base of the cochlea.

Nuclear staining

Nuclear staining was performed to illustrate tissue structures and to determine the mode of cell death. Following the staining procedures described above, nuclei were labeled with propidium iodide (5 μg/ml in 10 mM PBS, Invitrogen) or 4′,6-diamidino-2′-phenylin dole, dihydrochloride (DAPI, 1 mg/ml in 10 mM PBS, ThermoFisher Scientific, Waltham, MA, USA) at room temperature for 10 min. Specimens were mounted on slides containing anti-fade (ProLong Gold Antifade Mountant, Invitrogen).

Assessment of caspase activity

Caspase activity was assessed with a caspase-8 assay kit (CaspGLOW Red Active Caspase-8, 1:30 in solvent, BioVision, Milpitas, California, USA). The staining was performed *in vivo* as described in our previous publication (Ding et al., 2007; Hu et al., 2008). Briefly, animals were anesthetized (ketamine, 100 mg/kg and xylazine, 10 mg/kg) and the auditory bulla was exposed. The posterior wall of the bulla was opened to access the round and oval windows. About 10 μl of the caspase staining solution was slowly perfused into the cochlea through the round window in 1 h. Excessive perilymph and caspase staining solution was allowed to exit freely via the oval window. After staining, the animals were sacrificed and the cochleae were perfused with 10 mM PBS and then with 10% formalin for fixation. The cochleae were incubated in the same fixative for 3 h. After the fixation, the cochleae were dissected to collect the whole-mount preparations for confocal microscopy.

Quantitative and qualitative analyses of macrophages

Immunolabeled tissues were first photographed using a fluorescence microscope (Leica Z6 APO Manual MacroFluo, 10× objective) equipped with a Leica DFC digital camera. Sites of interest were further examined and imaged using a Zeiss LSM 510 META confocal microscope (Carl Zeiss, Oberkochen, Germany). The entire length of the sensory epithelium was imaged and the images were processed using Adobe Photoshop CS6 for quantification of basilar membrane macrophages. Basilar membrane macrophages are located on the scala tympani side of the basilar membrane. Macrophages were identified based on their unique morphology and their numbers were quantified from apex to the base. In addition, the sizes of the macrophages were measured using Adobe Photoshop CS6. Specifically, we selected the ten largest macrophages in the apical and the basal section of the basilar membrane. These cells were manually outlined, and the area contained within each outlined cell was calculated. The areas of the ten cells were averaged per specimen to provide a single representative number for each individual cochlea.

Western blotting

Animals were sacrificed by CO_2 asphyxiation, decapitated and their cochleae were quickly removed from the skull, dissected in 10 mM PBS and the cochlear tissues containing the sensory epithelia and the lateral walls were collected. Tissues from one cochlea of an animal were used to generate one sample. The collected tissues were immediately placed in liquid nitrogen and stored at −80 °C before further processing. For protein extraction, the tissues were homogenized in 50 μl of ice-cold lysis buffer containing 0.1% SDS with a tissue grinder (Kimble Chase, Vineland, NJ, USA). The homogenate was then centrifuged for 15 min at 12,000 rpm at 4 °C and then the supernatant was collected. The protein concentrations were determined by the Bradford method (Bio-Rad Laboratories, Hercules, CA, USA). Tissue homogenate proteins were then resolved by SDS-PAGE. Equivalent protein (30 μg protein/lane) and a pre-stained molecular weight marker (SeeBlue Plus2 Pre-Stained Protein Ladder, ThermoFisher Scientific) were loaded into the wells of 12% polyacrylamide gels in a mini-gel apparatus (Mini-PROTEAN II, Bio-Rad). Electrophoresis was conducted at 100 V for 120 min. The protein was then transferred onto polyvinylidene difluoride membranes (0.45 μm pore size, Millipore). The membrane was blocked with 5% skimmed milk for 60 min, rinsed in a mixture of PBS and tween-20 and incubated overnight at 4 °C with a sestrin 2 polyclonal antibody (1:1000, ProteinTech) and Glyceraldehyde-3-phosphate dehydrogenase (GAPDH) Rabbit antibody (1:1000, Cell Signaling, Danvers, MA, USA). Immunoreactive bands were detected using an anti-rabbit HRP-conjugated secondary antibody (1:1500, Cell Signaling) and visualized using chemiluminescent substrates (Pierce ECL Western Blotting Substrate, ThermoFisher Scientific). GAPDH was used as a reference protein for normalization of SESN2 protein expression. The intensities of the bands were measured using a scanning densitometer (ChemiDoc Imaging System, Bio-Rad).

Real-time quantitative polymerase chain reaction (RT-qPCR)

The transcriptional expression levels of SESN2, six proinflammatory genes (Il6, Tnf, Ccl2, Ccl3, Ccl4, Il1b) and three reference genes (Gapdh, Actin, Hprt and Hsp90) were examined using a pre-developed TaqMan gene expression probe assay (Applied Biosystems). *Sesn2* mRNA was examined in C57BL/6J control mice of 4–6 weeks and 5 months of age to determine how aging affects the transcriptional expression of SESN2. The expression of the proinflammatory genes was examined in 4–6-week- old C57BL/6J control and KO mice to determine the effect of the loss of *Sesn2* on the levels of proinflammatory activity.

Animals were deeply anesthetized with CO_2 and decapitated. The cochleae were quickly collected; the bony shell toward the middle ear cavity was opened and then placed in an RNA stabilization reagent (RNAlater, Qiagen, Valencia, CA, USA). The cochleae were dissected in the RNA stabilization reagent to collect the apical portion (top 30% of the cochlear turn) and the basal portion (40% to 80% from the apex) of the sensory epithelium and lateral wall tissues. Tissue from one cochlea was used to generate one apical and one basal sample. The isolated tissues were transferred to RNase-free PCR tubes and stored at −80 °C before RNA extraction.

Total RNA was isolated using the RNeasy Micro Kit (Qiagen) as per manufacturer's instruction. The concentration of isolated total RNA was measured with a NanoDrop

instrument (NanoDrop 1000, ThermoFisher Scientific). The isolated total RNA was reverse transcribed into cDNA using a High Capacity cDNA Reverse Transcription Kit (Applied Biosystems). Synthesized cDNA was mixed with a target gene probe and a TaqMan Universal PCR Master Mix (ThermoFisher Scientific) and transferred to a 96-well plate. RT-qPCR was performed on a MyIQ-two color real time PCR detection system (Bio-Rad).

Data analyses

ABR measurements—The threshold was defined as the lowest intensity of the acoustic stimulus that reliably elicited a detectable response. Two-way ANOVAs were performed to compare the thresholds among different experimental conditions across the different frequencies. The identification of significant ANOVA effects and interactions were followed by an appropriate post hoc pairwise comparison.

Sensory cell damage—Specimens were observed with a florescence microscope (Leica Z6 APO Manual MacroFluo, 10× objective) to identify OHC lesions. Missing phalloidin staining in the cuticular plates of OHCs was considered as missing cells. The number of missing OHCs was counted and the distribution of the cell loss is presented using a cochleogram. One-way or two-way ANOVAs were performed to compare the numbers of missing OHCs among groups.

Quantitative analysis of basilar membrane macrophages—Basilar membrane macrophages are defined as the macrophages that reside on the scala tympani side of the basilar membrane. Our previous study showed that these macrophages express both CD45 and F4/80 (Yang et al., 2015). In the current study, we used their unique morphology using CD45 immunoreactivity to identify these cells. All specimens were observed with a fluorescence microscope (Leica Z6 APO Manual MacroFluo, 10× objective). Macrophage numbers were quantified from the apex to the base of the sensory epithelium. Student's *t* tests or two-way ANOVAs were performed to compare the total number of macrophages between groups. The sizes of macrophages were compared using Student's *t* test.

Western blotting—Western blot band intensities were expressed quantitatively as arbitrary optical density units, which correspond to the target protein band intensity divided by the GAPDH signal intensity for the same sample. The differences among groups were analyzed using Student's *t* test.

RT-qPCR—Transcriptional expressions of the genes of interest were analyzed using a relative quantification method (Livak and Schmittgen, 2001). The expression level of a target gene was first normalized to the expression level of reference genes to generate the ΔCt value. Then ΔΔCt was calculated with the formula: ΔΔCt = ΔCt (experimental condition) – ΔCt (control condition). Paired Student's *t* test was performed to compare the changes in gene expression.

All data were presented as mean ± 1 standard deviation. The significance of changes or differences between conditions was examined using GraphPad Prism 5 (Graphpad Software Inc., La Jolla, CA, USA) or SigmaStat (Systat Software, San Jose, CA, USA). Normative data and equal variance tests were performed for all statistical analyses. If these two criteria

were not satisfied, non-parametric tests were performed. Multiple comparisons were corrected for using either the Bonferroni *t*-test or the Mann Whitney U-test. Results were considered statistically significant if the p-value was less than 0.05.

RESULTS

SESN2 is expressed in the cochlear sensory epithelium

We examined SESN2 immunolabeling in the cochleae of C57BL/6J control mice ($n = 3$) using whole-mount preparations. SESN2 immunoreactivity was observed in both sensory cells and supporting cells in the organ of Corti (Fig. 2A and B). Immunoreactivity was strongest in the cytoplasm of OHCs. In contrast, SESN2 immunoreactivity was absent in the cochleae of *Sesn 2* KO mice (Fig. 2C and D). Expression of SESN2 in sensory cells suggests it plays a role in the stress response and homeostasis of these cells.

Reduction in SESN2 expression with the increase of age

C57BL/6J mice exhibit early onset ARHL starting around 4–8 weeks at higher frequencies and spreading to lower frequencies with advancing age over the next 12–15 months (Ison et al., 2007; Someya et al., 2009). To determine whether cochlear degeneration is associated with changes in SESN2 expression its expression levels were evaluated in 4–6 week old C57BL/6J mice that have no significant sensory cell loss and 5-month-old mice that have basal turn sensory cell loss. First, we examined the mRNA level of *Sesn2* using RT-qPCR. The apical portion (0–30% from the apex) and basal portion (50–100% from the apex) of the cochlea were evaluated. Compared to the young samples ($n = 4$ biological replicates), the 5-month samples ($n = 4$ biological replicates) displayed a 70% decrease in *Sesn2* mRNA level (Fig. 3A; Student's *t* test, $t(6) = -2.534$; $P = 0.044$).

Next, we examined the protein expression level of SESN2 using Western blotting. We collected the cochlear tissues containing both the sensory epithelium and the lateral wall from young and 5-month cochleae ($n = 4$). Again, we found a significant reduction in SESN2 expression in the 5-month samples compared to 4–6-week-old mice (Fig. 3B, Student's *t* test, $t(4) = 2.280$; $P = 0.042$). Together, these observations revealed a reduction in SESN2 expression at both the transcriptional and protein levels with the increase in age.

Loss of SESN2 function potentiates age-related cochlear degeneration

Given the involvement of SESN2 in the cochlear aging, we sought to determine its functional role in cochlear homeostasis and pathology. We used *Sesn2* KO mice to determine the impact of the loss of *Sesn2.* In the samples of the sensory epithelia of KO mice, *Sesn2* transcriptional level assessed by RT-qPCR was either undetectable or extremely low with a Ct value greater than 38 compared to Ct values of 30 in C57BL/6J control mice. This confirms the absence of *Sesn2* in the KO mice.

We first examined the effect of loss of *Sesn2* on ABR function in *Sesn2* KO compared to C57BL/6J control mice in three age groups. Compared with the thresholds of young C57BL/6 mice (4–6 weeks, $n = 7$), thresholds in both the 3-month ($n = 7$) and the 5-month animals ($n = 7$) C57BL/6 mice were poorer at the higher frequencies (Fig. 4A; two-way

ANOVA, $F(2,82) = 33.4$, $P < 0.001$; Bonferroni *t*-test, $P < 0.05$ at 4 kHz for the 3- and 5-month groups, $P < 0.001$ at 32 and 48 kHz for the 3- and 5-month groups). This early onset high-frequency hearing loss is consistent with the pattern of hearing dysfunction reported in previous studies of C57BL/6J control mice (Ison et al., 2007; Someya et al., 2009). In *Sesn2* KO mice, we found a similar pattern of high-frequency hearing deterioration with age (Fig. 4B). However, the KO mice displayed greater threshold deterioration with age compared to C57BL/6J control mice (Fig. 4B). Importantly, at the age of 4–6 weeks ($n = 5$), thresholds in *Sesn2* KO were significantly greater than in C57BL/6J control mice at 4, 32, and 48 kHz with the threshold differences being 11 ± 2.7 dB for 4 kHz, 20.9 ± 22.1 dB for 32 kHz and 32.3 ± 5.8 dB at 48 kHz (Fig. 4C, two-way ANOVA, $F(1,46) = 42.3$, $P < 0.001$; Bonferroni *t*-test, $P = 0.021$ for the comparison at 4 kHz, $P < 0.001$ for the comparisons at 32 and 48 kHz). The high-frequency thresholds in the KO mice were greater than in the C57BL/6J control mice at 3-months ($n = 7$) (Fig. 4D, two-way ANOVA, $F(1,60) = 19.5$, $P < 0.001$, $P = 0.001$ for 32 kHz and $P = 0.008$ for 48 kHz) and 5 months ($n = 4$) (Fig. 4E, twoway ANOVA, $F(1,41) = 15.4$, $P < 0.001$; Bonferroni *t*-test, $P = 0.001$ for 32 kHz). This result suggests that loss of SESN2 exacerbates ARHL.

We compared hair cell loss in C57BL/6 versus *Sesn2* KO. In C57BL/6J control mice, only a few missing OHCs were found in young cochleae (4–6 weeks, $n = 13$, Fig. 5A). In 5-month ($n = 7$) cochleae, OHC loss observed was confined to the basal region of the cochlea (Fig. 5B). The age-matched *Sesn2* KO mice displayed greater sensory cell loss than C57BL/6J control of the same age (Fig. 5E, F and G). At 4–6 weeks when C57BL/6J control mice exhibited virtually no sensory cell loss, the *Sesn2* KO mice ($n = 8$) displayed OHC lesions at the basal extreme of the sensory epithelium (Fig. 5C) and the lesion expanded with age as seen in 5 month cochleae (Fig. 5D, $n = 5$). Unlike the base-dominated OHC loss in the C57BL/6J mice, the KO mice displayed broad OHC lesion from the apical to basal regions at 5 months (Fig. 5G). The presence of a second more apical lesion demonstrates the greater susceptibility of *Sesn2* KO mice to the age-related sensory cell pathogenesis. Additionally, compared with the C57BL/6J control mice, the average percentages of missing cells per cochlea in the KO mice were significantly higher at all ages (Fig. 5H, two-way ANOVA, $F(1,35) = 82.2$ $P = 0.033$; Bonferroni *t*-test, $P < 0.001$ at 4–6 weeks, $P = 0.009$ at 3-months, $P < 0.001$ at 5 months). These results suggest that loss of *Sesn2* accelerates the rate of age-related sensory cell degeneration.

To explore the mechanisms of hair cell death, we examined the nuclear morphology of hair cells. Age-related sensory cell degeneration undergoes an apoptotic process characterized by nuclear condensation (Yang et al., 2012, 2013). We examined the nuclear morphology in aged KO mice (5 months, $n = 3$) and found elevated propidium iodide fluorescence, a sign of the early stage of nuclear condensation, and a marked decrease in nuclear size and nuclear condensation, morphological features consistent with apoptosis (Fig. 6B). To evaluate the nature of apoptosis, we examined caspase-8 labeling associated with the extrinsic cell death pathway (Boatright and Salvesen, 2003; Eldadah and Faden, 2000; Nicotera et al., 2003). In a KO mouse, caspase-8 fluorescence was found in OHCs in cochlear section that displayed sensory cell lesions (Fig. 6C). Together, these observations suggest that OHC apoptosis is mediated in part by the extrinsic cell death pathway in the cochleae of *Sesn2* KO mice.

SESN2 deficiency provokes immune responses in the sensory epithelium

To determine the effects of the loss of *Sesn2* on the sensory epithelium, we examined inflammatory activity in the sensory epithelium by examining the transcriptional expression of five proinflammatory genes (*Tnf, Ccl2, Ccl3, Ccl4, Il1b*) that have been implicated in inflammatory responses in the cochlea in response to stresses (Cai et al., 2014a; Vethanayagam et al., 2016). We collected cochlear tissues containing the sensory epithelium and the lateral wall from C57BL/6J control mice ($n = 5$ biological replicates) and *Sesn2* KO mice ($n = 4$ biological replicates) at 4–6 weeks of age when early sensory cell degeneration took place in the KO mice. For the apical samples, we found a clear upregulation for all genes in the KO samples when the genes were analyzed individually. However, the differences between the KO and the C57BL/6J control samples for individual genes were not statistically significant. When the examined genes were analyzed as a group, we found that overall expression in the KO mice was significantly higher than that observed in the C57BL/6J control mice (Fig. 7A; Student's *t* test, $t(8) = 3.7$, $^{**}P = 0.006$). For the basal samples, no significant differences were detected (Fig. 7B; Student's *t* test, $t(8) = -0.243$, $P = 0.814$).

To determine why the difference in inflammatory molecule gene expression only occurred in the apical section of the cochlea, we examined the phenotypical properties of basilar membrane macrophages. Our previous investigations demonstrated that the basilar membrane macrophages, which reside on the scala tympani side of the basilar membrane, are able to respond to sensory cell degeneration and can serve as an internal sensor during sensory epithelium inflammation (Frye et al., 2016; Yang et al., 2015). In those studies, we observed that apical and basal macrophages have distinctly different morphologies, with apical macrophages having a dendritic shape and basal macrophages being stingray-like and ameboid shaped. Therefore, we compared the apical and basal macrophage populations in C57BL/6J controls and KO mice.

Apical macrophages are present in the apical 0–30% of the cochlea. In C57BL/6J control mice, these macrophages exhibited a slender body with multiple long, thin dendritic projections (Fig. 8A and D). A similar morphology was observed in KO mice (Fig. 8B and E). However, the macrophage bodies were enlarged in the KO mice, particularly in the 5-month KO mice that displayed very enlarged cell bodies filled with vacuoles (Fig. 8E). To quantify our observations, we compared the macrophage size between the C57BL/6J control and KO mice. In young mice (4–6 weeks), the average size of macrophages in KO mice was slightly larger than that in C57BL/6J control mice ($n = 5$ cochleae, $383.6 \pm 85.81\ \mu m^2$ vs. $306.4 \pm 78.17\ \mu m^2$; Student's *t* test, $t(18) = 2.104$; $^{***}P = 0.0497$; Fig. 8C). There was a significant increase in macrophage area in aged KO mice ($n = 5$ cochleae, $1247 \pm 234.4\ \mu m^2$) compared to aged C57BL/6J control mice ($n = 5$ cochleae, $701.2 \pm 92.29\ \mu m^2$; Student's *t* test, $t(18) = 2.104$; $^{*}P = 0.0497$; Fig. 8F). This pattern of morphological transformation suggests the activation of macrophages in KO mice, consistent with other organ systems (McWhorter et al., 2013; Steinman and Cohn, 1973; Streit et al., 1988).

In the basal 50–100% of the sensory epithelium, macrophage shapes were irregular or globular. At 4–6 weeks, the basal macrophages are tree-trunk-like or ameboid in shape and some had thin, short projections (Fig. 9A and B). At 5 months, the macrophages become

largely ameboid (Fig. 9D and E). There were no significant differences in the shapes of the macrophages between C57BL/6J control and KO mice. However, the sizes of macrophages were different between the C57BL/6J control and KO mice. In young mice (4–6 weeks, n = 5 cochleae), we found a slight, but significant, increase in the macrophage size in KO mice (1118 ± 151.7 μm^2) compared to C57BL/6J control mice (884.4 ± 65.57 μm^2; Student's t test, t (18) = 4.476; ***P <0.001; Fig. 9C). Similarly, at 5-months, we found a significant increase in the macrophage size in KO mice (n = 5 cochleae; 1574 ± 209.7 μm^2) compared to C57BL/6J control mice (1079 ± 127.8 μm^2; Student's t test, t (18) = 6.376; ***P <0.001; Fig. 9F). This observation suggests that KO mice have greater macrophage activity in the sensory epithelium.

We quantified the numbers of the basilar membrane macrophages in young and aged C57BL/6J control (n = 6 cochleae for 4–6 weeks and n = 4 cochleae for 5 months) and KO mice (n = 3 cochleae for 4–6 weeks and n = 3 cochleae for 5 months). In both the young and 5-month groups, the total numbers of macrophages were significantly higher in the KO mice compared to the age-matched C57BL/6J control mice (Fig. 10A for the 4–6 week groups, Student's t test, t (8) = 3.44; P = 0.004; Fig. 10B for the 5-month groups, Student's t test, t (4) = 5.27; P = 0.006). These results are consistent with previous findings of more macrophages in the liver of KO mice compared to C57BL/6J control mice (Park et al., 2014). Moreover, we found that the increase was more prominent in the basal portion of the sensory epithelium in 5-month mice (Fig. 10C, two-way ANOVA, F (1,10) = 17.2, P = 0.002; Bonferroni t-test, P < 0.001 for 4–6 weeks vs. 5 months in the basal region). Together, these observations suggest that KO mice have enhanced macrophage activity particularly in the basal portion of the basilar membrane.

DISCUSSION

The genetic background of individuals plays an essential role in susceptibility to auditory dysfunction. Multiple genes contribute to the maintenance of cochlear integrity and/or in the generation of cochlear pathology. These genes participate in various cellular functions, such as outer hair cell motility (SLC26A5) (Liu et al., 2003), antioxidant detoxification (Sod1) (McFadden et al., 2001) and inflammation (Tnf) (Cai et al., 2014b; Fujioka et al., 2006; Hu et al., 2009). Sestrins are a family of stress-inducible proteins that have been implicated in tissue responses to stress (Budanov et al., 2002; Velasco-Miguel et al., 1999). They protect cells from stresses such as oxidative DNA damage (Lee et al., 2013) and act as anti-aging molecules for decelerating the development of age-associated pathologies. Here, for the first time, we identified *Sesn2* as a novel gene for the maintenance of cochlear homeostasis and the suppression of age-related degeneration in the cochlea. We found the expression of SESN2 in the organ of Corti cells. This expression decreased with age when sensory cell degeneration takes place, suggesting an age-related reduction in SESN2 expression could be caused by the Ahl allele in B6 background mice. Importantly, we found that loss of SESN2 exacerbates both age-related auditory dysfunction and sensory cell pathogenesis. Together, these results implicate SESN2 as an important cochlear molecule in sensory cell homeostasis.

The mechanisms by which SESN2 affects cochlear hair cell loss is unclear. Our observations suggest that caspase-8-mediated apoptosis play a key step in sensory cell degeneration. Age-related sensory cell degeneration is known to be apoptotic (Hu et al., 2008; Jiang et al., 2007) and this mode of cell death is caused, in part, by overproduction of ROS (Wong and Ryan, 2015). Sestrins function as antioxidants for ROS neutralization, suppressing apoptosis and protecting tissues from age-related degeneration (Kim et al., 2014; Perez and Bao, 2011). The lack of SESN2 sensitizes cells to stress-induced apoptosis whereas SESN2 expression in SESN2 deficit cells protects against cell death (Ben-Sahra et al., 2013). These observations suggest that modulating the cellular redox balance is a cellular mechanism by which SESN2 affects sensory cell homeostasis.

We found evidence for increased inflammatory activity in *Sesn2* KO mice compared to C57BL/6J mice. There was increased expression of proinflammatory molecules and the activity of basilar membrane macrophages in *Sesn2* KO mice. This observation is consistent with previous findings that expressions of genes associated with inflammatory are altered during age-related cochlear degeneration and accompanied by an increase in circulating macrophages (Boggs et al., 1986; Strohacker et al., 2012; Tra et al., 2011). Because excessive inflammation is detrimental to the structure and function of the cochlea (Raphael, 2002), our findings suggest that cochlear inflammation may interact with sensory cell damage and compromise the sensory cell survival. Sensory cell degeneration was prominent in the base of both C57BL/6J control mice and KO mice. However, KO mice displayed significantly greater sensory cell lesions in the base of the cochlea at 4–6 weeks. While the onset of sensory cell pathogenesis in the base of the cochlea of C57BL/6J control mice was delayed, the lesion started from the extreme base of the cochlea and progressed toward the apex with increasing age. This basal vulnerability has been observed in other forms of cochlear pathogenesis, including noise-induced and ototoxicity-provoked cochlear damage. The presence of augmented proinflammatory activity in the base of the cochlea could contribute to basal turn susceptibility. We found that at a young age, both the KO and C57BL/6J control mice have ameboid macrophages in the basal end of the cochlea, which is distinct from the dendritic or branched phenotypes in the middle and apical regions of the cochlea. Given that the ameboid morphology represents proinflammatory activation of macrophages; our data suggest the presence of proinflammatory activity in the basal end of the cochlea in both strains of mice at an early age. This could explain why significant difference in the expression of proinflammatory molecules was not found in the basal regions between the two strains of mice. However, we found increased expression of proinflammatory molecules in the apical section of the cochlea in KO mice consistent with the view that increased proinflammatory activity precedes the onset of sensory cell pathogenesis (Frye et al., 2017).

We propose two possible explanations as to why *Sesn2* KO mice develop greater inflammatory activity. First, *Sesn2* KO mice could have greater oxidative stress in sensory cells and this enhanced oxidative activity could provoke a stronger inflammatory response of the cochlea (Wong and Ryan, 2015). Secondly, *Sesn2* KO mice display early onset sensory cell death. The toxic cellular components released by dying sensory cells could cause an increased inflammatory response. This view is supported by a previous finding that SESN2 expression prevents inflammatory responses initiated by the activation of Toll-like receptors

(Tlr) in macrophages (Yang et al., 2016). Tlr are a group of membrane sensor molecules that can detect both extrinsic molecules from bacteria and intrinsic molecules from damaged cells. Our recent studies demonstrated that Tlr4, a member of the Tlr family, participates in noise-induced cochlear inflammation (Cai et al., 2014a; Vethanayagam et al., 2016). Together, our finding of augmented inflammation is potentially important because modulation of inflammation has the potential to improve sensory cell microenvironment and thereby slow the progression of cochlear degeneration in ARHL.

In summary, our results reveal that SESN2 is expressed in the mouse cochlea and its expression is down-regulated with advancing age. Importantly, loss of SESN2 expression accelerates cochlear dysfunction and sensory cell degeneration and augments the immune response. These results implicate SESN2 as a novel gene in sensory cell homeostasis and age-related degeneration. Although the knockout effect of SESN2 is considered to be the cause of the phenotypic differences observed between the control and KO mice, we acknowledge that the results might be contributed by other genetic variants due to the fact that the controls are not littermate controls. Additionally, the effects of SESN2 deficiency may interact with the effects of the *Ahl* allele in KO mice with the C57BL/6J background and this interaction may contribute to our current physiological and histological findings. Therefore, the overall conclusion needs to be taken with consideration of these factors. Further studies are needed to elucidate the molecular mechanisms responsible for SESN2 regulation of cochlear inflammatory activity during sensory cell pathogenesis.

Acknowledgments

The authors thank Drs. Senthilvelan Manohar and Fen Xiong (UB Center for Hearing and Deafness) and Drs. Yina Ma, Nanhu Quan and Jilin Wang (UB Department of Pharmacology and Toxicology) for their contributions to the research. This research was supported by UB University Honors College Research and Creativity Fund and UB Center for Undergraduate Research and Creative Activities (CZ), Chinese National Science Foundation under the award number 81528005 (WS), National Institute on Aging of the National Institutes of Health under award numbers R21AG044820 and R01AG049835 (JL), National Heart, Lung and Blood Institute of the National Institute of Health under award number P01HL051971 (JL), National Institute of General Medical Sciences of National Institutes of Health under award number P20GM104357 (JL), American Diabetes Association Innovative Basic Science Grant 1-17-IBS-296 (JL), National Institute on Deafness and Other Communication Disorders of the National Institutes of Health under award numbers R01DC011808, R01DC014452, R01DC014693 (RS), R03DC011840, R01DC012552, R01DC014437 (SS) and R01DC010154 (BHH).

Abbreviations

ABR	auditory brainstem response
ARHL	age-related hearing loss
DAPI	4′,6-diamidino-2′-phenylindole, dihydrochloride
GAPDH	glyceraldehyde-3-phosphate dehydrogenase
KO	knockout
OHC	outer hair cell
PBS	phosphate-buffered saline

ROS	reactive oxygen species
RT-qPCR	quantitative reverse transcriptase-polymerase chain reaction
Tlr	Toll-like receptor

References

Ben-Sahra I, Dirat B, Laurent K, Puissant A, Auberger P, Budanov A, Tanti JF, Bost F. Sestrin2 integrates Akt and mTOR signaling to protect cells against energetic stress-induced death. Cell Death Differ. 2013; 20:611–619. [PubMed: 23238567]

Bielefeld EC, Tanaka C, Chen GD, Henderson D. Age-related hearing loss: is it a preventable condition? Hear Res. 2010; 264:98–107. [PubMed: 19735708]

Boatright KM, Salvesen GS. Caspase activation. Biochem Soc Symp. 2003:233–242. [PubMed: 14587296]

Boggs D, Patrene K, Steinberg H. Aging and hematopoiesis. VI. Neutrophilia and other leukocyte changes in aged mice. Exp Hematol. 1986; 14:372–379. [PubMed: 3519265]

Budanov AV, Karin M. P53 target genes sestrin1 and sestrin2 connect genotoxic stress and mTOR signaling. Cell. 2008; 134:451–460. [PubMed: 18692468]

Budanov AV, Shoshani T, Faerman A, Zelin E, Kamer I, Kalinski H, Gorodin S, Fishman A, Chajut A, Einat P, Skaliter R, Gudkov AV, Chumakov PM, Feinstein E. Identification of a novel stress-responsive gene Hi95 involved in regulation of cell viability. Oncogene. 2002; 21:6017–6031. [PubMed: 12203114]

Budanov AV, Sablina AA, Feinstein E, Koonin EV, Chumakov PM. Regeneration of peroxiredoxins by p53-regulated sestrins, homologs of bacterial AhpD. Science. 2004; 304:596–600. [PubMed: 15105503]

Budanov AV, Lee JH, Karin M. Stressin' Sestrins take an aging fight. EMBO Mol Med. 2010; 2:388–400. [PubMed: 20878915]

Cai Q, Wang B, Coling D, Zuo J, Fang J, Yang S, Vera K, Hu BH. Reduction in noise-induced functional loss of the cochleae in mice with pre-existing cochlear dysfunction due to genetic interference of prestin. PLoS ONE. 2014; 9:e113990. [PubMed: 25486270]

Cai Q, Vethanayagam RR, Yang S, Bard J, Jamison J, Cartwright D, Dong Y, Hu BH. Molecular profile of cochlear immunity in the resident cells of the organ of Corti. J Neuroinflammation. 2014; 11:173. [PubMed: 25311735]

Ding D, Jiang H, Wang P, Salvi R. Cell death after co-administration of cisplatin and ethacrynic acid. Hear Res. 2007; 226:129–139. [PubMed: 16978814]

Eldadah BA, Faden AI. Caspase pathways, neuronal apoptosis, and CNS injury. J Neurotrauma. 2000; 17:811–829. [PubMed: 11063050]

Finkel T, Holbrook NJ. Oxidants, oxidative stress and the biology of ageing. Nature. 2000; 408:239–247. [PubMed: 11089981]

Frisina DR, Frisina RD, Snell KB, Burkard R, Walton JP, Ison JR. Auditory temporal processing during aging. Funct Neurobiol Aging. 2001:565–579.

Frye MD, Yang W, Zhang C, Xiong B, Hu BH. Dynamic activation of basilar membrane macrophages in response to chronic sensory cell degeneration in aging mouse cochleae. Hear Res. 2016

Frye MD, Yang W, Zhang C, Xiong B, Hu BH. Dynamic activation of basilar membrane macrophages in response to chronic sensory cell degeneration in aging mouse cochleae. Hear Res. 2017; 344:125–134. [PubMed: 27837652]

Fujioka M, Kanzaki S, Okano HJ, Masuda M, Ogawa K, Okano H. Proinflammatory cytokines expression in noise-induced damaged cochlea. J Neurosci Res. 2006; 83:575–583. [PubMed: 16429448]

Hu BH, Yang WP, Bielefeld EC, Li M, Chen GD, Henderson D. Apoptotic outer hair cell death in the cochleae of aging Fischer 344/NHsd rats. Hear Res. 2008; 245:48–57. [PubMed: 18778762]

Hu BH, Cai Q, Manohar S, Jiang H, Ding D, Coling DE, Zheng G, Salvi R. Differential expression of apoptosis-related genes in the cochlea of noise-exposed rats. Neuroscience. 2009; 161:915–925. [PubMed: 19348871]

Ison JR, Allen PD, O'Neill WE. Age-related hearing loss in C57BL/6J mice has both frequency-specific and non-frequency-specific components that produce a hyperacusis-like exaggeration of the acoustic startle reflex. J Assoc Res Otolaryngol. 2007; 8:539–550. [PubMed: 17952509]

Jiang H, Talaska AE, Schacht J, Sha SH. Oxidative imbalance in the aging inner ear. Neurobiol Aging. 2007; 28:1605–1612. [PubMed: 16920227]

Kamogashira T, Fujimoto C, Yamasoba T. Reactive oxygen species, apoptosis, and mitochondrial dysfunction in hearing loss. Biomed Res Int. 2015; 2015:617207. [PubMed: 25874222]

Kapahi P, Zid B. TOR pathway: linking nutrient sensing to life span. Sci Aging Knowledge Environ. 2004:PE34. [PubMed: 15356349]

Khullar S, Babbar R. Presbycusis and auditory brainstem responses: a review. Asian Pacific J Trop Dis. 2011:150–157.

Kim GT, Lee SH, Kim JI, Kim YM. Quercetin regulates the sestrin 2-AMPK-p38 MAPK signaling pathway and induces apoptosis by increasing the generation of intracellular ROS in a p53-independent manner. Int J Mol Med. 2014; 33:863–869. [PubMed: 24535669]

Lee DJ, Kang SW. Reactive oxygen species and tumor metastasis. Mol Cells. 2013; 35:93–98. [PubMed: 23456330]

Lee JH, Bodmer R, Bier E, Karin M. Sestrins at the crossroad between stress and aging. Aging (Albany NY). 2010; 2:369–374. [PubMed: 20606249]

Lee JH, Budanov AV, Karin M. Sestrins orchestrate cellular metabolism to attenuate aging. Cell Metab. 2013; 18:792–801. [PubMed: 24055102]

Linehan E, Fitzgerald DC. Ageing and the immune system: focus on macrophages. Eur J Microbiol Immunol (Bp). 2015; 5:14–24. [PubMed: 25883791]

Liu XZ, Yan D. Ageing and hearing loss. J Pathol. 2007; 211:188–197. [PubMed: 17200945]

Liu XZ, Ouyang XM, Xia XJ, Zheng J, Pandya A, Li F, Du LL, Welch KO, Petit C, Smith RJ, Webb BT, Yan D, Arnos KS, Corey D, Dallos P, Nance WE, Chen ZY. Prestin, a cochlear motor protein, is defective in non-syndromic hearing loss. Hum Mol Genet. 2003; 12:1155–1162. [PubMed: 12719379]

Livak KJ, Schmittgen TD. Analysis of relative gene expression data using realtime quantitative PCR and the 22DDCT method. Methods. 2001:402–408. [PubMed: 11846609]

McFadden SL, Ohlemiller KK, Ding D, Shero M, Salvi RJ. The influence of superoxide dismutase and glutathione peroxidase deficiencies on noise-induced hearing loss in mice. Noise Health. 2001; 3:49–64. [PubMed: 12689448]

McWhorter FY, Wang T, Nguyen P, Chung T, Liu WF. Modulation of macrophage phenotype by cell shape. Proc Natl Acad Sci U S A. 2013; 110:17253–17258. [PubMed: 24101477]

Morrison A, Chen L, Wang J, Zhang M, Yang H, Ma Y, Budanov A, Lee JH, Karin M, Li J. Sestrin2 promotes LKB1-mediated AMPK activation in the ischemic heart. Faseb J. 2015; 29:408–417. [PubMed: 25366347]

Nicotera TM, Hu BH, Henderson D. The caspase pathway in noise-induced apoptosis of the chinchilla cochlea. J Assoc Res Otolaryngol. 2003; 4:466–477. [PubMed: 14534835]

Ohlemiller KK. Mechanisms and genes in human strial presbycusis from animal models. Brain Res. 2009; 1277:70–83. [PubMed: 19285967]

Ohlemiller, KK., Frisina, RD. Auditory trauma, protection, and repair. US: Springer; 2008. Age-related hearing loss and its cellular and molecular bases; p. 145-194.

Orr WC, Sohal RS. Extension of life-span by overexpression of superoxide dismutase and catalase in Drosophila melanogaster. Science. 1994; 263:1128–1130. [PubMed: 8108730]

Park HW, Park H, Ro SH, Jang I, Semple IA, Kim DN, Kim M, Nam M, Zhang D, Yin L, Lee JH. Hepatoprotective role of Sestrin2 against chronic ER stress. Nat Commun. 2014; 5:4233. [PubMed: 24947615]

Perez P, Bao J. Why do hair cells and spiral ganglion neurons in the cochlea die during aging? Aging Dis. 2011; 2:231–241. [PubMed: 22396875]

Quan N, Sun W, Wang L, Chen X, Bogan JS, Zhou X, Cates C, Liu Q, Zheng Y, Li J. Sestrin 2 prevents age-related intolerance to ischemia and reperfusion injury by modulating substrate metabolism. Faseb J. 2017

Raphael Y. Cochlear pathology, sensory cell death and regeneration. Br Med Bull. 2002; 63:25–38. [PubMed: 12324382]

Ro SH, Xue X, Ramakrishnan SK, Cho CS, Namkoong S, Jang I, Semple IA, Ho A, Park HW, Shah YM, Lee JH. Tumor suppressive role of sestrin2 during colitis and colon carcinogenesis. Elife. 2016; 5:e12204. [PubMed: 26913956]

Sena LA, Chandel NS. Physiological roles of mitochondrial reactive oxygen species. Mol Cell. 2012; 48:158–167. [PubMed: 23102266]

Sohal RS, Weindruch R. Oxidative stress, caloric restriction, and aging. Science. 1996; 273:59–63. [PubMed: 8658196]

Someya S, Prolla TA. Mitochondrial oxidative damage and apoptosis in age-related hearing loss. Mech Ageing Dev. 2010; 131:480–486. [PubMed: 20434479]

Someya S, Xu J, Kondo K, Ding D, Salvi RJ, Yamasoba T, Rabinovitch PS, Weindruch R, Leeuwenburgh C, Tanokura M, Prolla TA. Age-related hearing loss in C57BL/6J mice is mediated by Bak-dependent mitochondrial apoptosis. Proc Natl Acad Sci U S A. 2009; 106:19432–19437. [PubMed: 19901338]

Staecker H, Zheng QY, Van De Water TR. Oxidative stress in aging in the C57B16/J mouse cochlea. Acta Otolaryngol. 2001; 121:666–672. [PubMed: 11678164]

Stanfel MN, Shamieh LS, Kaeberlein M, Kennedy BK. The TOR pathway comes of age. Biochim Biophys Acta. 2009; 1790:1067–1074. [PubMed: 19539012]

Steinman RM, Cohn ZA. Identification of a novel cell type in peripheral lymphoid organs of mice. I. Morphology, quantitation, tissue distribution. J Exp Med. 1973; 137:1142–1162. [PubMed: 4573839]

Streit WJ, Graeber MB, Kreutzberg GW. Functional plasticity of microglia: a review. Glia. 1988; 1:301–307. [PubMed: 2976393]

Strohacker K, Breslin WL, Carpenter KC, McFarlin BK. Aged mice have increased inflammatory monocyte concentration and altered expression of cell-surface functional receptors. J Biosci. 2012; 37:55–62. [PubMed: 22357203]

Tadros SF, D'Souza M, Zhu X, Frisina RD. Gene expression changes for antioxidants pathways in the mouse cochlea: relations to age-related hearing deficits. PLoS ONE. 2014; 9:e90279. [PubMed: 24587312]

Tanaka C, Coling DE, Manohar S, Chen GD, Hu BH, Salvi R, Henderson D. Expression pattern of oxidative stress and antioxidant defense-related genes in the aging Fischer 344/NHsd rat cochlea. Neurobiol Aging. 2012; 33(1842):e1–e14. [PubMed: 22244089]

Tra Y, Frisina RD, D'Souza M. A novel high-throughput analysis approach: immune response-related genes are upregulated in age-related hearing loss. Open Access Bioinf. 2011:107–122.

Velasco-Miguel S, Buckbinder L, Jean P, Gelbert L, Talbott R, Laidlaw J, Seizinger B, Kley N. PA26, a novel target of the p53 tumor suppressor and member of the GADD family of DNA damage and growth arrest inducible genes. Oncogene. 1999; 18:127–137. [PubMed: 9926927]

Vethanayagam RR, Yang W, Dong Y, Hu BH. Toll-like receptor 4 modulates the cochlear immune response to acoustic injury. Cell Death Dis. 2016; 7:e2245. [PubMed: 27253409]

Waris G, Ahsan H. Reactive oxygen species: role in the development of cancer and various chronic conditions. J Carcinogenesis. 2006:14.

Wei JL, Fu ZX, Fang M, Guo JB, Zhao QN, Lu WD, Zhou QY. Decreased expression of sestrin 2 predicts unfavorable outcome in colorectal cancer. Oncol Rep. 2015; 33:1349–1357. [PubMed: 25572852]

Wong AC, Ryan AF. Mechanisms of sensorineural cell damage, death and survival in the cochlea. Front Aging Neurosci. 2015; 7:58. [PubMed: 25954196]

Yang WP, Guo WW, Liu HZ, Xu Y, Chen L, Hu BH. Age-related changes in the ratio of Mcl-1/Bax expression in the rat cochlea. Acta Otolaryngol. 2012; 132:123–132. [PubMed: 22201517]

Yang WP, Xu Y, Guo WW, Liu HZ, Hu BH. Modulation of Mcl-1 expression reduces age-related cochlear degeneration. Neurobiol Aging. 2013; 34:2647–2658. [PubMed: 23790646]

Yang W, Vethanayagam RR, Dong Y, Cai Q, Hu BH. Activation of the antigen presentation function of mononuclear phagocyte populations associated with the basilar membrane of the cochlea after acoustic overstimulation. Neuroscience. 2015; 303:1–15. [PubMed: 26102003]

Yang S, Cai Q, Vethanayagam RR, Wang J, Yang W, Hu BH. Immune defense is the primary function associated with the differentially expressed genes in the cochlea following acoustic trauma. Hear Res. 2016; 333:283–294. [PubMed: 26520584]

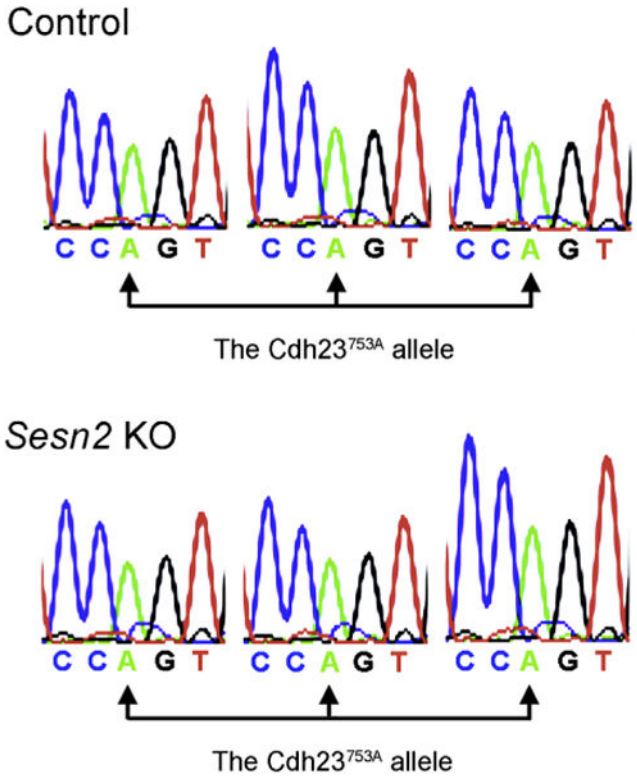

Fig. 1.

Genotyping of Cdh23 gene showing the same genotype between the control and *Sesn2* KO mice. The *Cdh23* gene was sequenced in three control (C57BL/6J) and three *Sesn2* KO mice that had been backcrossed to C57BL/6J for at least 9 generations. Both the control and *Sesn2* KO animals have the *Cdh23*$^{753A/753A}$ genotype.

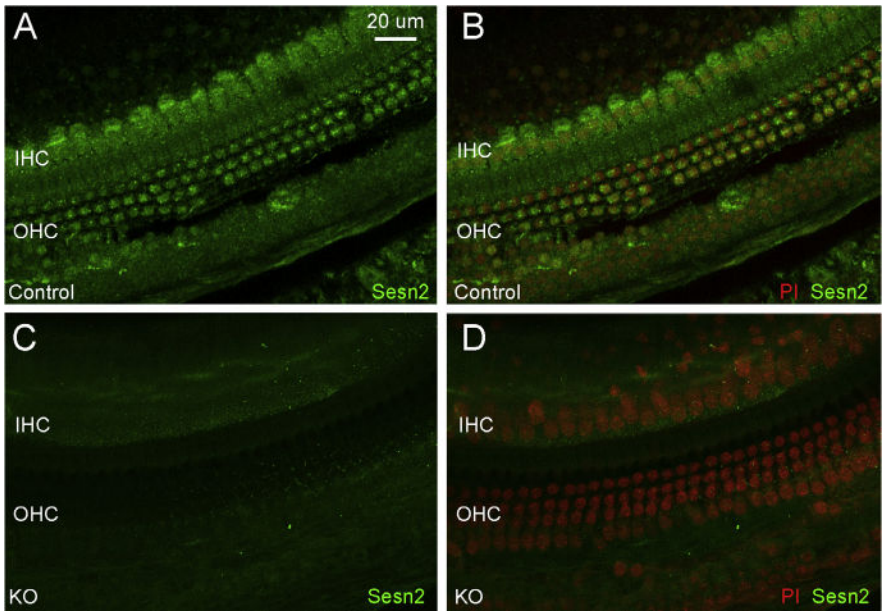

Fig. 2.

SESN2 immunoreactivity in the cochlear sensory epithelium. The samples were doubly stained with SESN2 (green fluorescence) and propidium iodide (PI, red fluorescence) for nuclei. (A) and (B) SESN2 immunoreactivity is present in both sensory cells and supporting cells of the organ of Corti. The images shown are the typical representation of the staining observed in three C57BL/6J control mouse cochleae. (C) and (D) SESN2 immunoreactivity is absent in the cochleae of *Sesn2* KO mice. OHC: outer hair cells; IHC: inner hair cells; PI: propidium iodide. Scale bar: 20 μm. (For interpretation of the references to colour in this figure legend, the reader is referred to the web version of this article.)

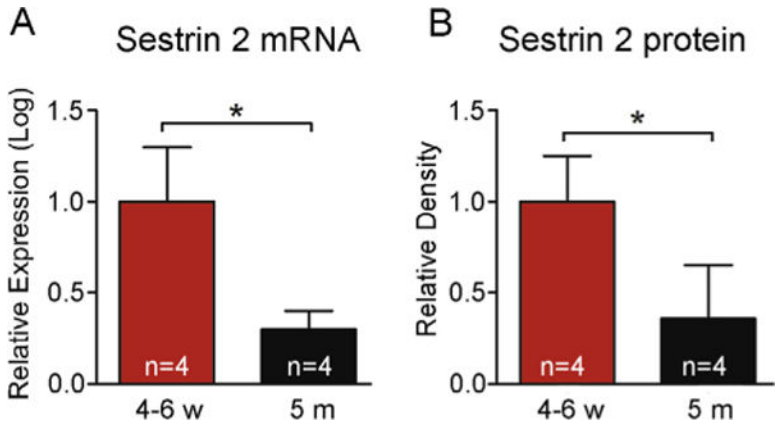

Fig. 3.

Reduction in SESN2 expression in the cochlea of C57BL/6J control mice with age. (A) Comparison of the *Sesn2* mRNA level between the 4–6-week-old and the 5-month-old C57BL/6J control mice. *Sesn2* mRNA expression levels were measured using RT-qPCR. The expression level is reduced in the 5-month group. *n* = the number of biological repeats. (B) Comparison of Western blotting band intensities, as arbitrary optical density units, of the SESN2 protein between the 4 and 6 week group and the 5-month group. GAPDH was used as the endogenous control. The band intensity is reduced in the 5-month group. These results indicate that SESN2 expression is reduced as the age increases. Bars represent standard deviations. $*P < 0.05$.

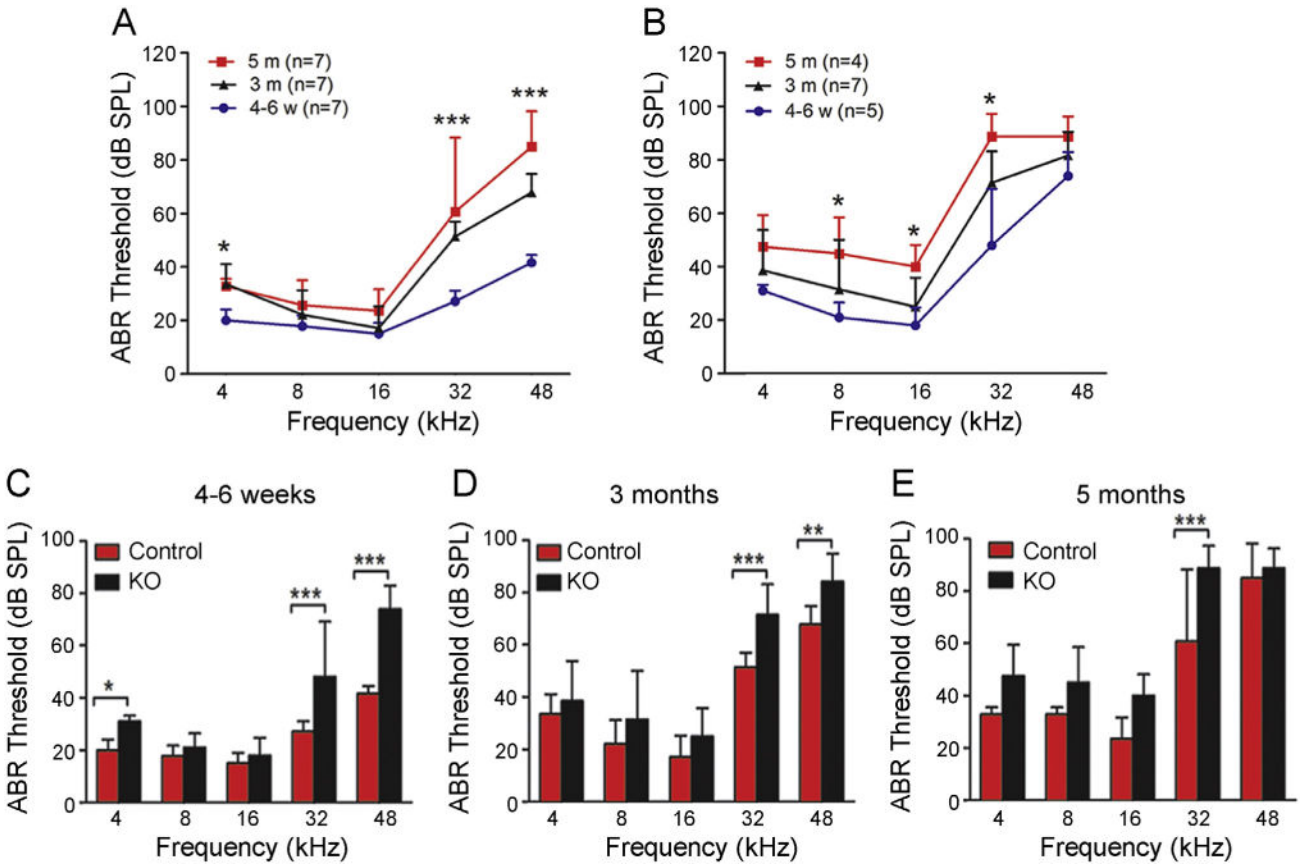

Fig. 4.

Comparison of age-related cochlear dysfunction in C57BL/6J control and *Sesn2* KO mice. (A) Comparison of ABR thresholds in C57BL/6J control mice among the three age groups (4–6 weeks, 3-months and 5 months) in five tested frequencies (4, 8, 16, 32 and 48 kHz). There is a progressive elevation in the thresholds at the high frequencies (32 and 48 kHz), ***$P < 0.001$ at 32 and 48 kHz for the 3- and 5-month groups. n = the number of cochleae. (B) Comparison of ABR thresholds in KO mice among the three age groups (4–6 weeks, 3-months and 5 months) in five tested frequencies (4, 8, 16, 32 and 48 kHz). There is significant elevation in the middle thresholds (8, 16 and 32 kHz), *$P < 0.05$ at 8 kHz for the 4–6 weeks and 5-month groups, at 16 kHz for the 4–6 weeks and 5-month groups and at 32 kHz for the 4–6 weeks and 5-month groups and the 4–6 weeks and 3-month groups. n = the number of cochleae. (C) Comparison of the ABR thresholds between the control and the KO mice at the age of 4–6 weeks. Significant differences are present at both the low (4 kHz) and the high frequencies (32 and 48 kHz), *$P = 0.021$, ***$P < 0.001$. (D) Comparison of the ABR thresholds between the C57BL/6J control and the KO mice at the age of 3 months. Significant differences are present in the high frequencies, ***$P = 0.001$ for 32 kHz and **$P = 0.008$ for 48 kHz. (E) Comparison of the ABR thresholds at the age of 5 months. A significant difference is present at 32 kHz, ***$P = 0.001$. Bars represent standard deviations. n = the number of cochleae.

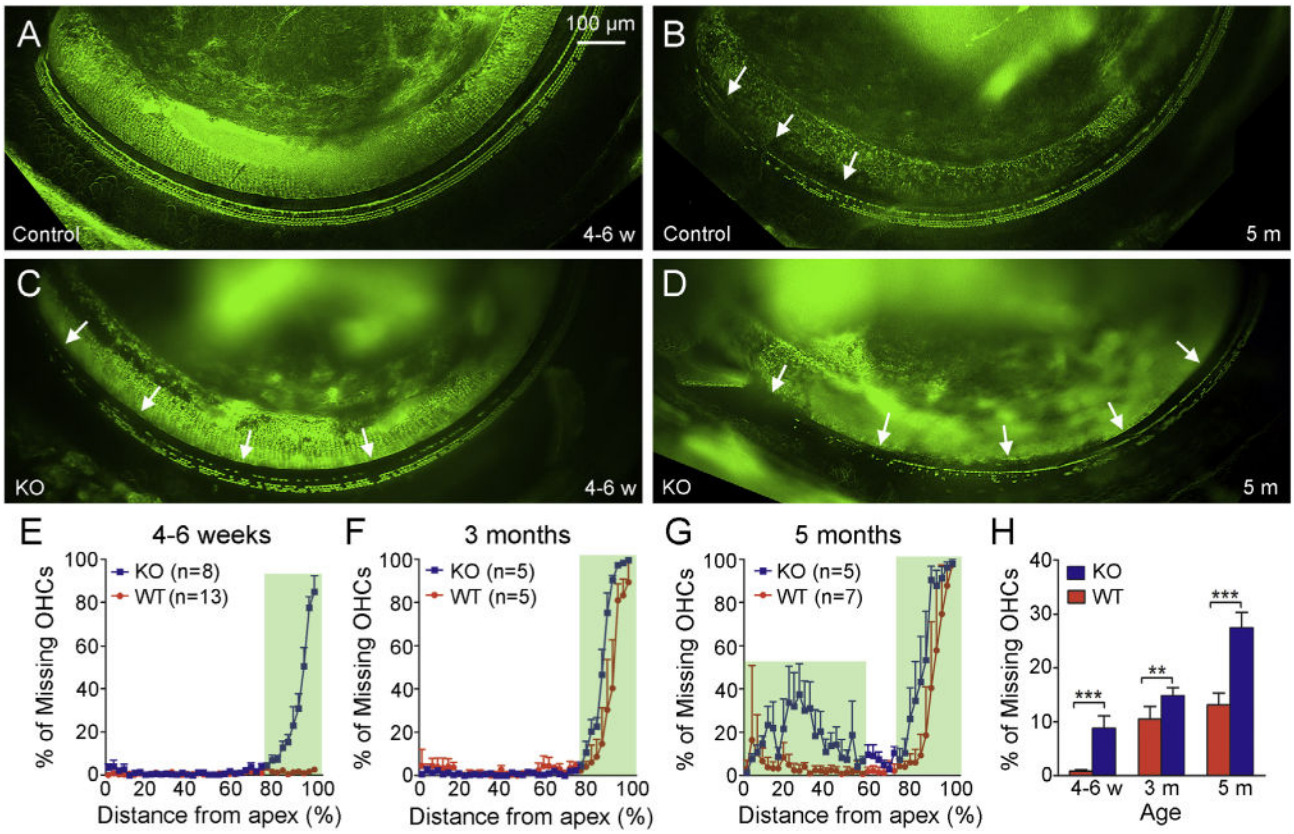

Fig. 5.

Comparison of age-related sensory cell degeneration between C57BL/6J control mice and *Sesn2* KO mice. (A) and (B) Typical images of F-actin staining of the cuticular plates of hair cells in C57BL/6J control mice showing the basal cochlear region where hair cell degeneration occurs. The young cochlea (4–6-week-old) shows little to no sensory cell loss (A). The 5-month-old cochlea displays loss of sensory cells (arrows) in the basal extreme around 90–100% distance from the apex (B). C and D: Typical images of F-actin staining of the cuticular plates of hair cells in KO mice showing the basal cochlear region where hair cell degeneration occurs. Sensory cell loss is already evident in the young cochlea (4–6 week old) pointed by the arrows at the basal extreme approximately 80–100% distance from the apex (C). At 5 months old, the KO cochlea exhibits extensive OHC loss in the basal extreme as pointed by the arrows (D). Cell loss is also evident in other parts of the cochlea (data not shown). Scale bars = 100 µm. E, F and G: Cochleogram showing the distribution of OHC loss along the basilar membrane in control and KO mice of 4–6 weeks (E), 3 months (F) and 5 months (G). The magnitude of OHC loss is presented using percentage of missing cells as function of the distance from the apex of the cochlea (in %). Notice that sensory cell loss starts from the basal end of the cochlea in both the control and KO mice. In both groups, OHC loss is confined in the basal section of the sensory epithelium at ages of 4–6 weeks and 3-months. However, the lesions expand to the apical region of the sensory epithelium at 5 months in KO mice. H: Comparison of the average percentage of missing OHC per cochlea between the C57BL/6J control and KO groups. The numbers of missing cells in the KO

mice are significantly higher in all age groups, ***$P < 0.001$; **$P < 0.01$. Bars represent standard deviations.

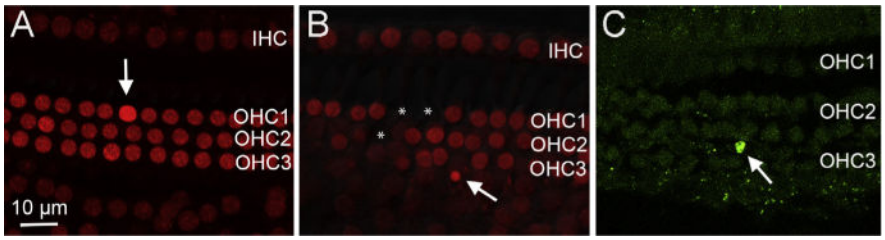

Fig. 6.

Induction of the apoptotic cell death pathway in the sensory epithelium of *Sesn2* KO mice. (A) and (B) Nuclear morphology illustrated by propidium iodide staining in 5-month cochleae. The arrow in A points to an early stage of nuclear condensation, characterized by an increase in propidium iodide florescence. The arrow in B points to an advanced stage of nuclear condensation, shown by an increase in propidium iodide florescence and a significant decrease in nuclear size. (C) Assessment of caspase-8 activity in a 5-month cochlea. The arrow points to caspase-8 activation. Both nuclear condensation and caspase activation are hallmarks of apoptosis. OHC1, OHC2 and OHC3 represent the first, second and third rows of OHCs, respectively. IHC represents inner hair cells. Images shown are typical representations of the staining observed in 5 cochleae. Scale bar: 10 μm.

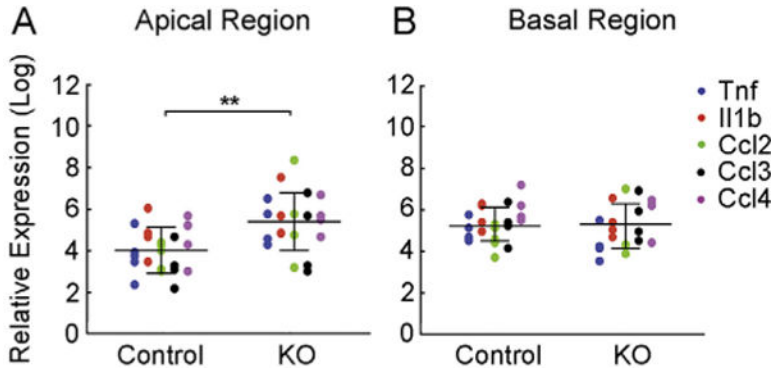

Fig. 7.

Comparisons of the mRNA expression levels of proinflammatory genes between *Sesn2* KO and C57BL/6J control mice. The expression of six proinflammatory genes (*Il6, Tnf, Ccl2, Ccl3, Ccl4*, and *Il1b*) were examined in cochlear tissues containing the sensory epithelium and the lateral wall collected from C57BL/6J control ($n = 5$ biological repeats) and knockout mice ($n = 4$ biological repeats) at 4–6 weeks of age. Among the six examined genes, five (*Tnf, Ccl2, Ccl3, Ccl4, Il1b*) were detected in the samples and the data are presented. The values presented are the relative expression levels that are normalized using reference genes. One dot represents one sample and one color represents one gene. (A) Comparison of the expression levels in the apical section of the cochlea (30% from the apex). The average expression level of the proinflammatory genes as a group is significantly higher in the KO mice than that in the C57BL/6J control mice, $^{**}P = 0.006$. (B) Comparison of the expression levels in the basal section of the cochlea (60–90% from the apex). The average expression level of the proinflammatory genes as a group is similar between the KO and the C57BL/6J control samples.

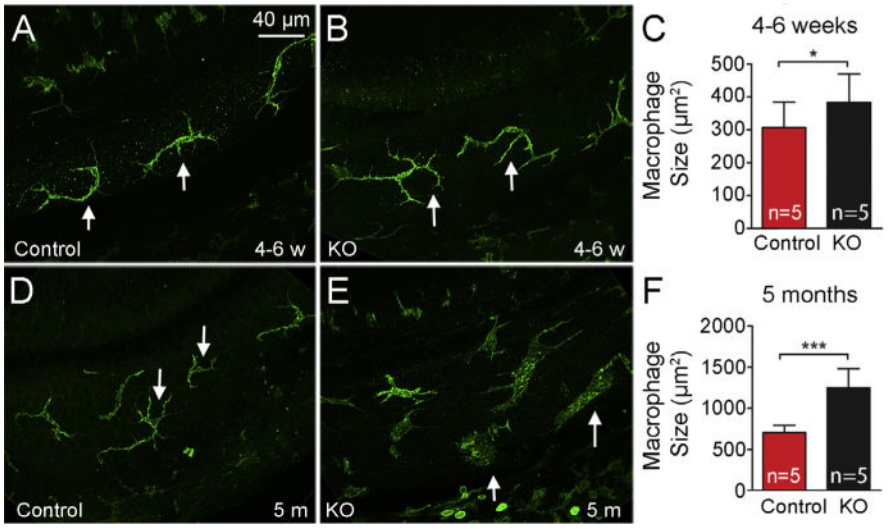

Fig. 8.

Typical morphology of basilar membrane macrophages in the apical section of the sensory epithelium (0–30% of the apex). The tissues were stained for CD45 immunoreactivity. (A) Macrophages in a young (4–6 week) C57BL/6J control mouse. These macrophages manifest slender bodies with multiple long, thin dendritic projections pointed by arrows. (B) Macrophages in a young KO mouse. Again, macrophages in this region exhibit the same dendritic morphology as those of the age-matched C57BL/6J control mouse. (C) Comparison of the sizes of apical macrophages between the C57BL/6J control ($n = 5$ cochleae) and KO ($n = 5$ cochleae) mice at the age of 4–6 weeks. There is a slight, but significant, increase in macrophage size in KO mice (383.6 ± 85.81 μm^2) compared to C57BL/6J control mice, ***$P = 0.0497$. (D) Macrophages in a 5-month control mouse. Macrophages maintain the dendritic phenotype seen in the young mice. (E) Macrophages in a 5-month KO mouse. The slim dendritic bodies become hypertrophied and the long processes are shortened. (F) Comparison of the sizes of apical macrophages between the C57BL/6J control ($n = 5$ cochleae) and KO ($n = 5$ cochleae) mice at the age of 5 months. There is a significant increase in the macrophage size in KO mice (1247 ± 234.4 μm^2) compared to C57BL/6J control mice, $P < 0.0001$. The enlargement of the cell body is a sign of activation in macrophages. Scale bar: 40 μm. Bars represent standard deviations.

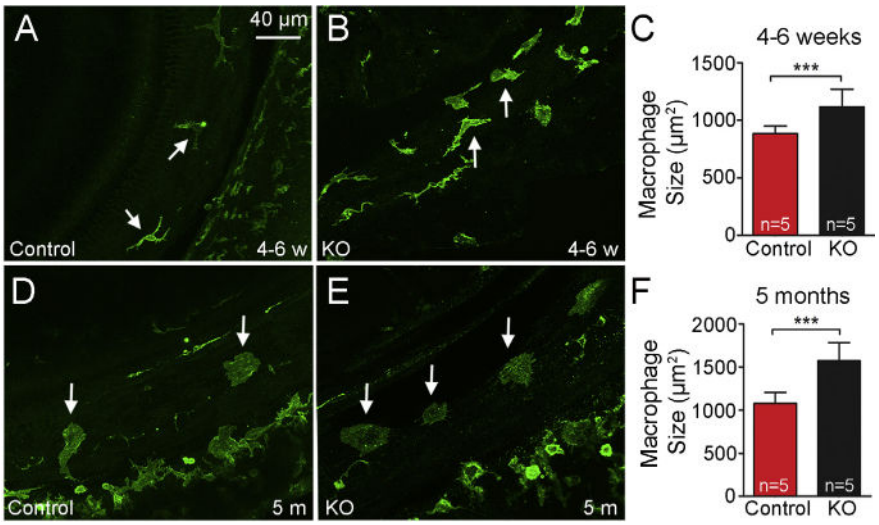

Fig. 9.

Typical morphology of basilar membrane macrophages in the basal section of the sensory epithelium (the basal 50% of the sensory epithelium). The tissues were stained for CD45 immunoreactivity. A and B: Macrophages in the basal end of the sensory epithelium in a C57BL/6J control (A) and a KO (B) mouse at the age of 4–6 weeks. The basal macrophages are tree trunk-like or ameboid in shape and have some thin and short projections (arrows). (C) Comparison of the sizes of basal macrophages between the C57BL/6J control ($n = 5$ cochleae) and KO ($n = 5$ cochleae) mice at the age of 4–6 weeks. There is a significant increase in the macrophage size in the KO mice (1118 ± 151.7 μm^2) compared to the C57BL/6J control mice, ***$P < 0.001$. D and E: Macrophages in the basal end of the sensory epithelium in a C57BL/6J control mouse (D) and a KO mouse (E) at the age of 5 months. Notice that ameboid macrophages, indicated by arrows, are present in both species. Noticeably, the macrophage projections seen in young mice disappear and the macrophages become completely ameboid. F: Comparison of the sizes of basal macrophages between the C57BL/6J control ($n = 5$ cochleae) and KO ($n = 5$ cochleae) mice at the age of 5 months. There is a significant increase in the macrophage size in the KO mice (1574 ± 209.7 μm^2) compared to the C57BL/6J mice, ***$P < 0.001$. Scale bar: 40 μm. Bars represent standard deviations.

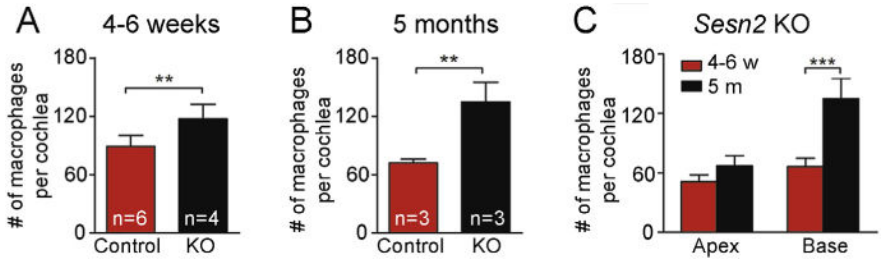

Fig. 10.

Sesn2 KO mice display an increase in the number of basilar membrane macrophages. (A) Comparison of the average numbers of basilar membrane macrophages per cochlea between the *Sesn2* KO mice ($n = 4$) and the control mice ($n = 6$) at the age of 4–6 weeks. The number of macrophages in the KO mice is significantly higher than that in the control mice, $^{**}P = 0.004$. (B) Comparison of the numbers of basilar membrane macrophages per cochlea between the KO mice ($n = 4$) and the control mice ($n = 4$) at the age of 5 months. Again, the average number of macrophages in the KO mice is significantly higher than that in the control mice, $^{**}P = 0.006$. (C) Comparison of the average numbers of macrophages per cochlea between the apical and the basal sensory epithelia of *Sesn2* KO mice at the ages of 4–6 weeks and 5-months. Notice that the age-related increase in the number of macrophages in the basal section is markedly higher than that in the apical section of the sensory epithelium, $^{***}P < 0.001$.